Volume 15
Number 32
28 August 2024
Pages 12619–13114

Chemical Science

rsc.li/chemical-science

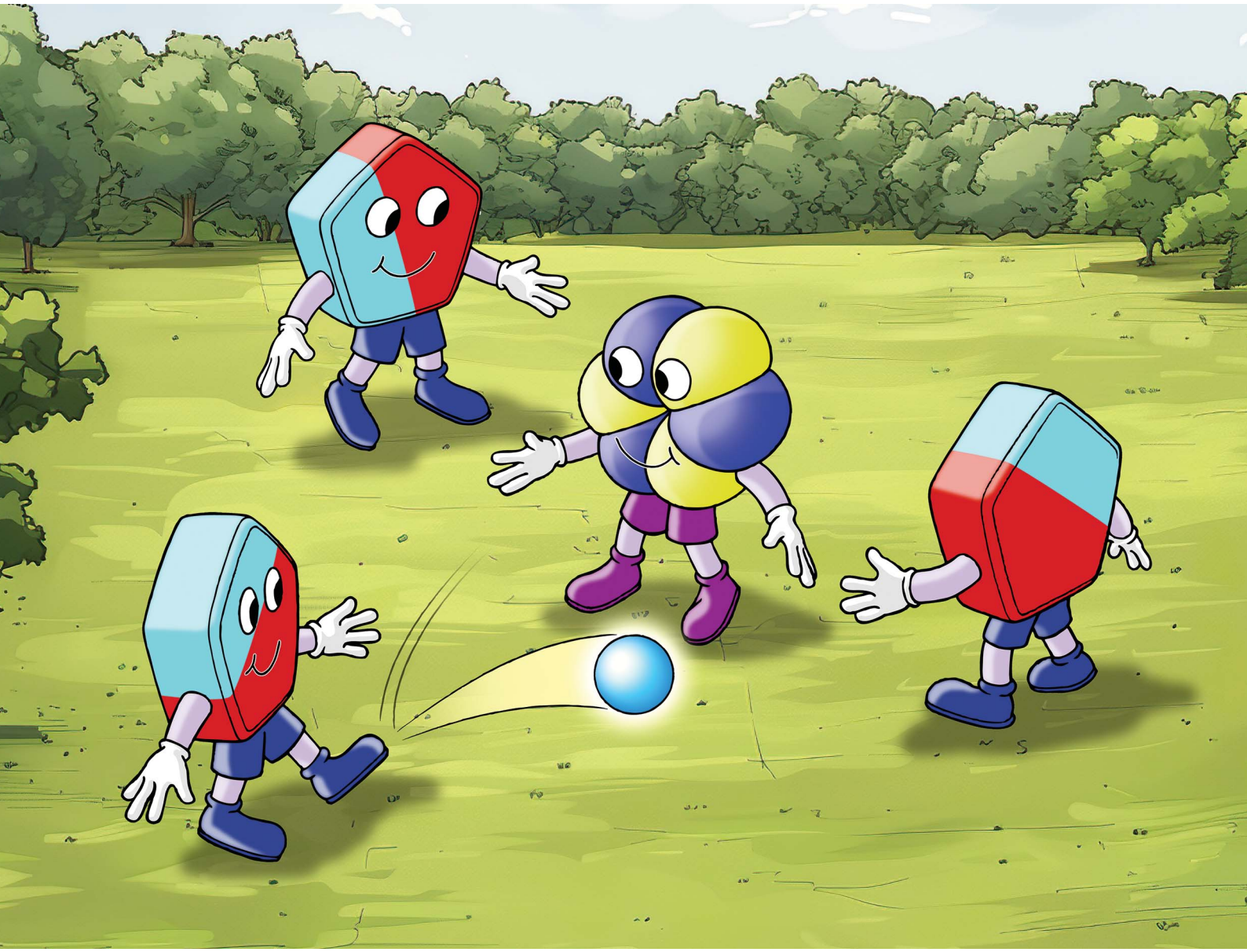

ISSN 2041-6539

ROYAL SOCIETY OF CHEMISTRY

EDGE ARTICLE

S. Olivia Gunther, Yusen Qiao *et al.*

4f-Orbital mixing increases the magnetic susceptibility of Cp'_3Eu

Chemical Science

ROYAL SOCIETY OF CHEMISTRY

EDGE ARTICLE

View Article Online
View Journal | View Issue

Cite this: *Chem. Sci.*, 2024, **15**, 12667

All publication charges for this article have been paid for by the Royal Society of Chemistry

Received 25th February 2024
Accepted 5th June 2024

DOI: 10.1039/d4sc01300j

rsc.li/chemical-science

4f-Orbital mixing increases the magnetic susceptibility of Cp'_3Eu†

S. Olivia Gunther, ‡[a] Yusen Qiao, ‡[a] Patrick W. Smith, [a] Sierra R. Ciccone,[b] Alexander S. Ditter,[a] Daniel N. Huh, §[b] Liane M. Moreau, [ac] David K. Shuh, [a] Taoxiang Sun, [d] Polly L. Arnold, [ae] Corwin H. Booth,[a] Wibe A. de Jong, [f] William J. Evans, [b] Wayne W. Lukens, Jr [a] and Stefan G. Minasian *[a]

Traditional models of lanthanide electronic structure suggest that bonding is predominantly ionic, and that covalent orbital mixing is not an important factor in determining magnetic properties. Here, 4f orbital mixing and its impact on the magnetic susceptibility of Cp'_3Eu ($Cp' = C_5H_4SiMe_3$) was analyzed experimentally using magnetometry and X-ray absorption spectroscopy (XAS) methods at the C K-, Eu $M_{5,4}$-, and L_3-edges. Pre-edge features in the experimental and TDDFT-calculated C K-edge XAS spectra provided unequivocal evidence of C 2p and Eu 4f orbital mixing in the π-antibonding orbital of a′ symmetry. The charge-transfer configurations resulting from 4f orbital mixing were identified spectroscopically by using Eu $M_{5,4}$-edge and L_3-edge XAS. Modeling of variable-temperature magnetic susceptibility data showed excellent agreement with the XAS results and indicated that increased magnetic susceptibility of Cp'_3Eu is due to removal of the degeneracy of the $^7F_1$ excited state due to mixing between the ligand and Eu 4f orbitals.

Introduction

The ability to harness the 4f-orbital anisotropies and magnetic susceptibilities of lanthanide (Ln) elements is key to their application in molecular magnetism, including as molecular qubits and single-molecule magnets (SMMs). For example, in the field of SMMs, chemists have developed ligand design principles[1–7] that facilitate subtle tuning of the crystal field, which in turn enhances magnetic anisotropy and the blocking temperature in single-ion[8–15] magnets. In addition to the 4f crystal field, lanthanide magnetic properties can be influenced by strong electron correlations, generating effects such as homogenous mixed valence with magnetic singlet formation and valence tautomerism.[16–22] However, the impact of covalent mixing between metal and ligand orbitals on the magnetic properties of trivalent lanthanide systems is typically small, compared to its more significant effect in actinide complexes[23–29] and in certain tetravalent lanthanide complexes.[30–36] The Ln 4f orbitals have limited radial extension, such that the effect of overlap between the 4f and ligand orbitals is much weaker than electron repulsion and spin–orbit coupling.[37] Covalent interactions between ligands and contracted 4f orbitals have been identified by recent theoretical and spectroscopic studies of Ln(III) compounds.[19–21,38–42] Despite this progress, it remains challenging to predict how charge transfer resulting from 4f orbital mixing will be manifested by changes in magnetic behaviour.[43]

Denning and coworkers previously quantified 4f shell covalency in Cp_3Yb in terms of charge-transfer from the ligand to the metal center using X-ray photoelectron spectroscopy (XPS), EPR (HYSCORE), and optical spectroscopies.[39,40] They hypothesized[40] that 4f shell covalency could also be significant in Cp_3Eu because, like Yb^{3+}, Eu^{3+} has a low-energy charge transfer state.[44] In fact, Cp'_3Eu (Cp' = trimethylsilylcyclopentadienyl) has a more positive redox potential relative to Cp'_3Yb (−1.07 V *vs.* −1.64 V, respectively),[45] and Eu and Yb have the most favourable third ionization potentials of the entire lanthanide series (24.92 ± 0.10 eV and 25.05 ± 0.03 eV, respectively).[46] Electron delocalization has been observed in Eu intermetallics; however, evidence of similar effects in molecules is limited.[47] 4f orbital mixing in an organometallic Eu(III) compound, $Cp_3Eu(THF)$, was illustrated by an unprecedentedly negative isomer shift in

[a]*Chemical Sciences Division, Lawrence, Berkeley National Laboratory, Berkeley, CA 94720, USA. E-mail: sgminasian@lbl.gov*

[b]*Department of Chemistry, University of California, Irvine, CA 92697, USA*

[c]*Department of Chemistry, Washington State University, Pullman, WA 99164, USA*

[d]*Institute of Nuclear and New Energy Technology, Tsinghua University, Beijing 100084, P. R. China*

[e]*Department of Chemistry, University of California, Berkeley, CA 94720, USA*

[f]*Computational Research Division, Lawrence Berkeley National Laboratory, Berkeley, CA 94720, USA*

† Electronic supplementary information (ESI) available: Experimental and computational methods, additional plots of XAS data for Cp'_3Eu (Ln = Eu, Gd, Yb). See DOI: https://doi.org/10.1039/d4sc01300j

‡ These authors contributed equally.

§ Present address: Department of Chemistry, University of Rhode Island, Kingston, RI 02881, USA.

its 151-Eu Mössbauer spectrum.[38] Laboratory XPS has recently been applied to study the electronic structures of Cp'_3Ln and [K(crypt)][Cp'_3Ln] (Ln = Gd, Eu, Sm, Tb), but spectral signatures for charge transfer were not observed.[48] Direct probes of 4f orbital mixing are needed to understand the relationship between charge transfer and magnetism in lanthanide organometallic complexes.

Studies of lanthanide and actinide organometallic compounds have shown that C K-edge XAS provides unique insight into the interactions between π systems and metal orbitals in specific valence orbitals.[49–51] We previously used a combination of C K-edge XAS and DFT to provide direct evidence of C 2p and Ce 4f orbital mixing in the δ-antibonding orbitals of $(C_8H_8)_2Ce$.[50] Here, we use C K-edge XAS and time dependent density functional theory (TDDFT) calculations to provide direct evidence of 4f orbital mixing in Cp'_3Eu. In addition, Eu L_3- and $M_{5,4}$-edge spectroscopies were used to show how the 4f-orbital mixing results in C 2p → Eu 4f charge transfer. Taken together with variable temperature magnetic susceptibility measurements, these spectroscopic evaluations reveal how 4f-orbital mixing can impact magnetism in lanthanide organometallic complexes.

Results and discussion

Ground state electronic structure

The following discussion of the molecular orbital interactions in Cp'_3Eu provides a framework for evaluating the experimental results. Because the electronic structures for $Ln(C_5R_5)_3$ (R=H or alkyl) are well established,[40,52–55] this discussion will focus on the metal-based orbitals that are relevant to the XAS experiments. Visual depictions comparing the effects of spin–orbit coupling, ligand field splitting, and coulombic repulsion have been published for f^1 systems,[7,56] but are not possible for Eu^{3+} due to the large number of states involved. Hence, an MO model for the interaction between 2p–π orbitals on the $[Cp'_3]^{3-}$ framework and the Eu 5d- and 4f-orbitals was constructed in pseudo-C_{3h} symmetry (Fig. 1).[40] In C_{3h}, the 5d orbitals on Cp'_3Eu transform as a′ (d_{z^2}), e′ (d_{xy} and $d_{x^2-y^2}$), and e″ (d_{xz} and d_{yz}), which form σ-, π-, and δ-bonding interactions with the equatorial Cp′ ligands. The Eu 4f orbitals transform as 2a′ + a″ + e′ + e″, most of which are best described as non-bonding. However, mixing between appropriate ligand orbitals and one of the 4f orbitals of a′ symmetry gives rise to a weakly π-antibonding MO.[58] Such mixing with the 4f orbitals can be described using an MO model by the linear combination of orbitals as:

$$\Psi^* = N\{\psi_{4f} - \lambda\psi_{Cp'\ \pi^*}\} \quad (1)$$

where N is a normalization constant, λ is the orbital mixing coefficient, and ψ_{4f} and $\psi_{Cp'\ \pi^*}$ are parent Eu and ligand-based wavefunctions. The MO model is advantageous because it describes how partial electron delocalization can occur in Cp'_3Eu due to specific types of orbital interactions (*e.g.*, σ, π, δ, φ), and is best-suited to interpret ligand-based spectroscopies such as C K-edge XAS (see below).

The MO model does not account for exchange interactions or core-hole induced charge transfer, among other effects associated with the multi-electron $4f^6$ configuration of a Eu^{3+} ion. Hence, the single-determinant MO wavefunction shown in eqn (1) can be rewritten using a many-electron, configuration interaction (CI) model,[50,59] where the ground state is expressed by a combination of two terms that differ only by one electron:

$$\Psi^* = N\{|4f^6\rangle + \lambda|4f^7\underline{L}\rangle\} \quad (2)$$

where $|4f^6\rangle$ is the ionic, Eu^{3+} configuration and $|4f^7\underline{L}\rangle$ describes the result of a ligand-to-metal electron transfer leading to reduction to Eu^{2+} and formation of a ligand hole ($\underline{L}$). Because the electrons are assumed to be fully localized, the CI model is better suited to interpret the metal-based Eu $M_{5,4}$- and L_3-edge XAS and magnetic measurements described below.

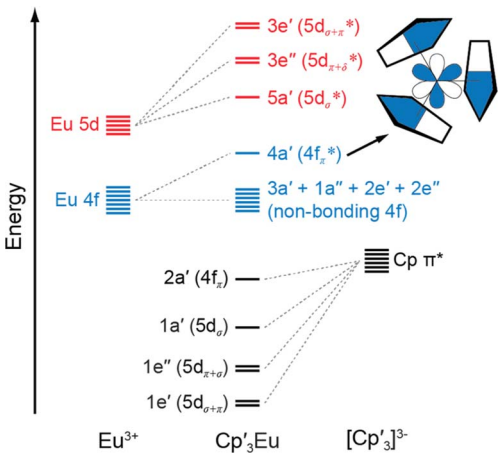

Fig. 1 A qualitative MO diagram of Cp_3Eu in C_{3h} symmetry. The inset shows the a′ antibonding interaction of metal f and ligand orbitals. The nodal characteristics of the $(Cp)_3^{3-}$ fragment relative to the metal atom are represented with common short-hand notation.[53,57]

Carbon K-edge XAS

C K-edge XAS spectra were collected with a scanning X-ray transmission microscope (STXM) on micron-scale crystallites of Cp'_3Eu (Fig. S4†).[58] This approach minimizes the saturation and self-absorption effects that commonly occur when using weakly penetrating incident radiation at low photon energies, and has been applied in the study of metal-carbon bonding for both d- and f-block systems.[49,50,60] The background-subtracted and normalized C K-edge spectrum of Cp'_3Eu is shown in Fig. 2A together with a curve-fit model. For the pre-edge region of the spectrum above 284 eV, the spectrum was fit using three Gaussian functions (refer to the ESI† for full details). The C K-edge spectrum of Cp'_3Eu also exhibited a small peak at low energy, which required a fourth Gaussian function at 283.6 eV. The presence of a transition in this energy range is unusual, since transitions below 284 eV have not been observed previously for a variety of 1st, 2nd, or 3rd row d-block metallocenes.[60–63] Because an equivalent low-energy peak was also not resolved in the C K-edge spectrum of $4f^7$ Cp'_3Gd (see Fig. S6†), we hypothesized that the peak at 283.6 eV was associated with transitions into MOs of 4f-parentage.

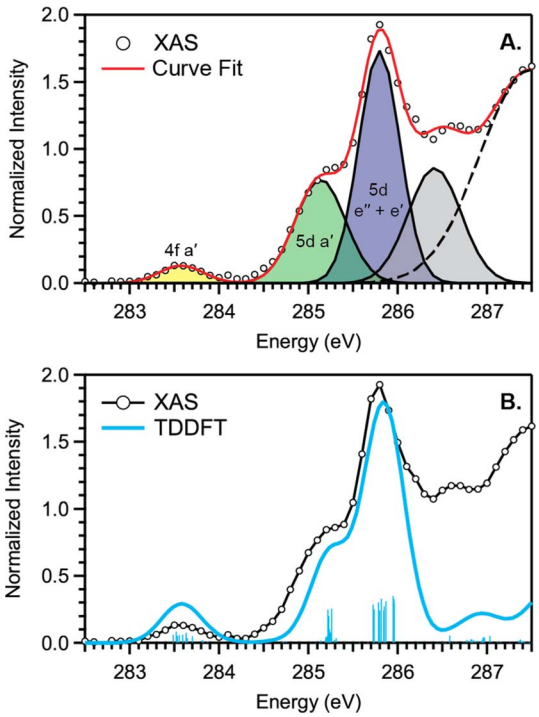

Fig. 2 (A) C K-edge XAS pre-edge of Cp'_3Eu (black circles), Gaussian functions (yellow, green, blue, and gray), and the sum of post-edge functions (dashed black trace) used to generate the total curve fit (red). (B) C K-edge XAS experimental data for Cp'_3Eu (black circles), the TDDFT-calculated spectrum (blue) and calculated transitions (vertical blue bars). The three main features are labeled with the acceptor MOs from the transition assignments.

To assign the pre-edge features in the C K-edge XAS of Cp'_3Eu, the spectrum was modelled using TDDFT implemented with NWChem and using the long-range corrected LC-PBE0 functional.[63] Fig. 2B shows that the experimental spectrum for Cp'_3Eu was well-reproduced with this computational method. Examination of the acceptor orbitals associated with a group of 15 transitions centered at 283.6 eV confirms that the low-energy feature is associated with transitions from the C 1s orbitals into the Eu–Cp′ π-antibonding 4f-orbital of a′ symmetry. Both the experimental and TDDFT calculated C K-edge spectrum agree regarding the relative location of the 4f and 5d orbitals; each show that the C 1s → a′ (4f–π) transition is 1.6 eV lower in energy than the lowest energy transition into the 5d manifold, C 1s → a′ (5d–σ). Moving to higher energy, the TDDFT calculations indicate that the next feature at 285.8 eV is associated with C 1s transitions into both the e″ ($5d^*_{\pi+\delta}$) and e′ ($5d^*_{\sigma+\pi}$) orbitals. These transitions are close in energy and not resolved individually in the experimental spectrum. The fourth feature observed at 286.4 eV was not well reproduced in the calculated spectrum; features in this energy range are likely associated with Rydberg-type orbitals that are not the unoccupied, antibonding counterpart to bonding orbitals that are occupied in the ground-state.[60]

The C K-edge pre-edge transitions described above have intensities that are weighted by the amount of C 2p character in the acceptor MO. Hence, the C K-edge XAS and TDDFT calculations provide evidence that C 2p and Eu 4f orbital mixing occurs specifically in the Eu–Cp′ π-antibonding orbitals of a′ symmetry. This assignment is consistent with the MO diagram derived experimentally from magnetometry (see below), which showed that the a′ MO is the most destabilized by the Cp′ ligand field. In this regard, Cp'_3Eu is similar to Cp_3Yb, which also exhibits significant orbital mixing in the partially occupied a′ orbital as shown by XPS and ADF-DFT calculations.[39,40] The consequence of mixing in the a′ MO is Cp′ → Eu charge transfer. In a configuration interaction (CI) model where the orbitals are localized, this mixing is manifested by a greater weight of the Eu^{2+} configuration, $4f^7\underline{L}$, where $\underline{L}$ represents a hole on one of the Cp′ ligands resulting from Cp′ π → 4f charge transfer.[22] Charge transfer is also reflected in the DFT calculation for Cp'_3Eu by the Lowdin spin population analysis, which provided a value of 6.32. This value exceeds the prediction of 6 for a Eu^{3+} ion and suggests that the weight of the Eu^{2+} CT configuration ($4f^{14}\underline{L}$) in the ground state is 32%.

Europium L_3- and $M_{5,4}$-edge XAS

Eu $M_{5,4}$-edge and L_3-edge XAS were obtained to provide further evidence of Cp′ π → 4f charge transfer interactions in Cp'_3Eu. Previous work has shown that $M_{5,4}$-edge and L_3-edge XAS are particularly useful techniques for probing 4f orbital mixing and charge transfer in tetravalent Ce, Pr, and Tb systems,[59,64–66] and in trivalent Sm, Eu, Tm, and Yb systems.[67–69] Both the Eu L_3 (2p → 5d) and $M_{5,4}$-edge (3d → 4f) spectroscopies probe electric-dipole allowed transitions from Eu core orbitals to empty or partially occupied valence orbitals.

Fig. 3 shows the background subtracted and normalized Eu $M_{5,4}$-edge XAS spectra for Cp'_3Eu compared to reference compounds for Eu^{2+} (Eu_2O_3) and Eu^{3+} ($EuAl_4$).[69] The spectra are split into low-energy M_5 ($3d_{5/2}$ → $4f_{7/2}$) and high-energy M_4 ($3d_{3/2}$ → $4f_{5/2}$) edges due to spin–orbit coupling with the 3d core

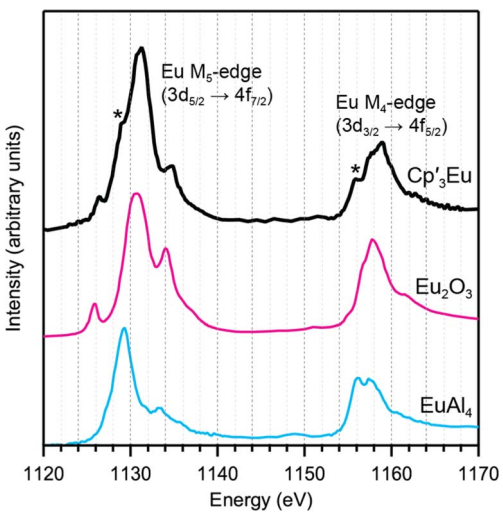

Fig. 3 $M_{5,4}$-edge spectrum for Cp'_3Eu (black) and references for Eu^{3+} (Eu_2O_3, magenta) and Eu^{2+} ($EuAl_4$, blue). Two features associated with Eu^{2+} character in the L_3-edge spectrum for Cp'_3Eu are highlighted with asterisks.

hole.[70,71] Both the M_5- and M_4-edges can also exhibit fine structure due to final-state multiplet splitting, with characteristic patterns based on the number of 4f electrons.[50,59,72,73] The spectrum of Cp'_3Eu consists of main M_5 and M_4 peaks centered at 1131.3 eV and 1158.9 eV, respectively, and fine structure that most clearly resembles the spectrum of Eu_2O_3.[70,71,74] However, additional features were also observed at 1129.1 and 1155.9 eV, which were not present in the spectrum for Eu_2O_3 but were coincident with the peak energies of the Eu^{2+} standard, $EuAl_4$.[69] In this regard the $M_{5,4}$-edge spectrum of Cp'_3Eu resembles that of mixed-valent Sm, Eu, and Tm solids, which have been described as superpositions of Ln^{3+} and Ln^{2+} subspectra.[68] Qualitatively, the presence of features attributable to both Eu^{2+} and Eu^{3+} configurations in the $M_{5,4}$-edge XAS of Cp'_3Eu provides further support for the existence of Cp′ $\pi \rightarrow$ 4f charge transfer interactions identified by C K-edge spectroscopy. However, the relatively low intensity of the Eu^{2+} features indicates that the Eu^{3+} configuration is likely a more dominant component of the ground state for Cp'_3Eu The spectrum of Cp'_3Eu is also distinct from the $M_{5,4}$-edge spectra of formally tetravalent Ce and Pr compounds, where the phenomenon of increased charge transfer in the final state causes emergence of satellite features at high energy relative to the main M_5 and M_4 peaks.[75] Theoretical models of $M_{5,4}$-edge spectra have been developed for certain f-element systems by using CI calculations,[50,59,72,76–80] but could not be performed at the time of this study due to challenges with incorporating charge transfer in the calculations.[81–83] More detailed theoretical and experimental investigation is needed to determine whether charge transfer satellite peaks are also present, but not resolved, in the $M_{5,4}$-edge spectra of Cp'_3Eu and some other Sm, Eu, and Tm molecules and solids.

Background-subtracted and normalized Eu L_3-edge XANES spectra of Cp'_3Eu and reference compounds Eu_2O_3 and Cp^*_2Eu are shown in Fig. 4. The spectra for Cp'_3Eu and Eu_2O_3 were similar in that both had the same white-line energy (6981.7 eV). However, Cp'_3Eu also exhibited a lower energy shoulder at *ca.* 6974 eV, which is similar to the white-line energies for Cp^*_2Eu (6975 eV) and other Eu^{2+} compounds.[84,85] The presence of two features in the Eu L_3-edge spectrum of Cp'_3Eu is reminiscent of the Yb L_3-edge spectra of Yb organometallic complexes[19–21] and the L_3-edge spectra of tetravalent Ce, Pr, and Tb compounds, which show a low-energy feature that is attributable to a charge-transfer configuration.[59] In analogy to these studies, we described the ground-state electronic structure of Cp'_3Eu with a CI model involving mixing between $4f^6 5d^0$ and $4f^7\underline{L}5d^0$ configurations. Then, at the Eu L_3-edge, transitions occur to $4f^6 5d^1$ and $4f^7\underline{L}5d^1$ final states, respectively. Based on this model, the low energy feature in the Eu L_3-edge spectrum of Cp'_3Eu was attributed to a $4f^7\underline{L}5d^0 \rightarrow 4f^7\underline{L}5d^1$ transition, and the main white-line feature was assigned to a $4f^6 5d^0 \rightarrow 4f^6 5d^1$. The *ca.* 6 eV peak separation was attributed to the difference in the number of 4f electrons that are available to screen the 5d electron from the Ln 2p core hole. The relative amount of $4f^7\underline{L}5d^0$ in the ground state was determined at 28(4)% by curve-fitting the spectrum (see Fig. S12 in the ESI†), which indicated that significant charge-transfer interactions are present Cp'_3Eu

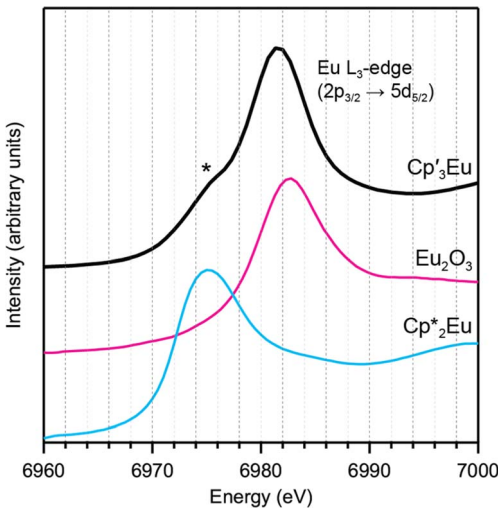

Fig. 4 L_3-edge spectrum for Cp'_3Eu (magenta) and references for Eu^{3+} (Eu_2O_3, dashed black) and Eu^{2+} (Cp^*_2Eu, dashed blue). A curve fit of the experimental data for Cp'_3Eu is provided in the ESI† (Fig. S12†). A shoulder associated with Eu^{2+} character in the L_3-edge spectrum for Cp'_3Eu is highlighted with an asterisk.

Yb L_3-edge XAS for were measured for comparison (see Fig. S13 in the ESI†), which indicated that the relative contribution of the corresponding $4f^{14}\underline{L}5d^0$ configuration to the ground-state was 0.11(3). The relative amount of $4f^7\underline{L}5d^0$ in the ground state, 0.28(4), is also referred to as n_f, the amount of additional 4f character introduced due to covalent bonding.

Magnetometry

Variable-temperature magnetic susceptibility data for Cp'_3Eu reported previously by Meihaus *et al.* (Fig. 5) was examined for evidence of charge transfer interactions.[86] At low temperature, Cp'_3Eu displays temperature independent paramagnetism (TIP) with χ equal to 0.13 emu mol^{-1}. At temperatures greater than ~10 K, the value of χ decreases as the first excited state becomes populated. Qualitatively, the magnetic susceptibility of an

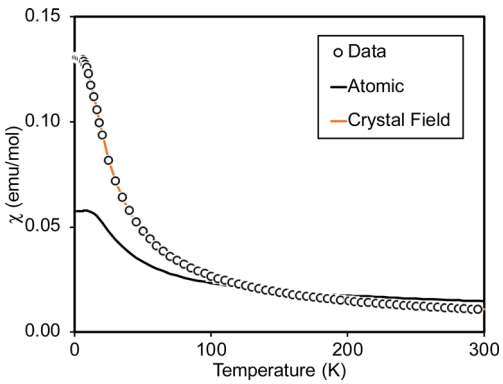

Fig. 5 Magnetic susceptibility of Cp'_3Eu (open circles). The fit using eqn (4) (free-ion model) is shown as a solid black line. The results of fitting the data using CONDON 3 (crystal field model with $k = 0.7$) is shown using an orange line.

isolated Eu^{3+} ion is straightforward. For a free Eu^{3+} cation, the term ^7F is split by spin–orbit coupling into seven states, ^7F_J, with $J = 0$–6. The energies of the states (E_J)[87,88] are:

$$E_J = \frac{\lambda}{2}[J(J+1)] \quad (3)$$

where λ is the spin–orbit coupling constant, which is 220 cm^{-1} (316 K) for a free Eu^{3+} ion.[89] Using a free-ion model of the electronic structure of Eu(III), the magnetic susceptibility of a Eu^{3+} ion may be calculated using van Vleck' theorem (eqn (4)):[87,88,90]

$$\chi = \frac{\sum_{J=0}^{J=6} \chi_J (2J+1) e^{-E_J/k_B T}}{\sum_{J=0}^{J=6} (2J+1) e^{-E_J/k_B T}} = \frac{N\mu_B{}^2}{Z}\left(\frac{A}{3\lambda}\right) \quad (4)$$

where:

$$A = 24 + \left(13.5\frac{\lambda}{k_B T} - 1.5\right)e^{\frac{-\lambda}{k_B T}} + \left(67.5\frac{\lambda}{k_B T} - 2.5\right)e^{\frac{-3\lambda}{k_B T}} + \left(189\frac{\lambda}{k_B T} - 3.5\right)e^{\frac{-6\lambda}{k_B T}} + \left(405\frac{\lambda}{k_B T} - 4.5\right)e^{\frac{-10\lambda}{k_B T}} + \left(742.5\frac{\lambda}{k_B T} - 5.5\right)e^{\frac{-15\lambda}{k_B T}} + \left(1228.5\frac{\lambda}{k_B T} - 6.5\right)e^{\frac{-21\lambda}{k_B T}} \quad (5)$$

and

$$Z = 1 + 3e^{-\lambda/k_B T} + 5e^{-3\lambda/k_B T} + 7e^{-6\lambda/k_B T} + 9e^{-10\lambda/k_B T} + 11e^{-15\lambda/k_B T} + 13e^{-21\lambda/k_B T} \quad (6)$$

At low temperature, only the $^7F_0$ orbital-singlet state is populated. This state displays temperature independent magnetism. As the temperature increases, the low-lying $^7F_1$ and $^7F_2$ excited states will be thermally populated, at which point the magnetic susceptibility, χ, becomes temperature dependent and starts to decrease.

However, the details of the magnetic susceptibility of Cp'_3Eu are not congruent with this free-ion treatment; both the χ value at 300 K and χ_{TIP} at low temperatures are larger than the values for the free Eu^{3+} cation and reported monomeric Eu(III) compounds. Both observations indicate that the lowest lying excited state is much lower in energy than typical for a Eu(III) complex.[87,88,91–96] Attempts to fit these data to a free-ion model using eqn (2) resulted in a very small λ value of 23 K which is an order of magnitude smaller than reported values for Eu(III) compounds (λ = 250–350 K) and is not realistic.[87,88,91–96] The free ion model fails due to its implicit assumption that the splitting of the J states by the crystal field is much smaller than the spin orbit coupling constant. The XAS results show that the ground state of Cp'_3Eu has a large contribution from a CT state, $4f^7\underline{L}5d^0$, due to mixing between the Eu 4f orbitals and the Cp′ orbitals with a′ symmetry. The magnitude of this interaction suggests that the splitting of the energies of the 4f-orbitals (and the J states) may be large enough to affect the variable temperature magnetic susceptibility of Cp'_3Eu

To examine this possibility, the magnetic susceptibility of Cp'_3Eu was modeled with crystal field theory using the program CONDON 3.[97] The crystal field parameters $B_0{}^2$, $B_0{}^4$, $B_0{}^6$, and $B_6{}^6$ were allowed to vary while spin–orbit coupling (ζ) and Slater repulsion were fixed at their starting values. In comparison to the crystal field parameters, the Slater parameters and ζ are less strongly affected by the ligands. Fits were also performed while allowing ζ to vary, but doing so increased the value of reduced chi-squared, $\chi_\nu{}^2$, which indicates that the models with ζ fixed at 1336 cm^{-1} better reproduced the data. The initial fit of the susceptibility reproduced the data well, but yielded crystal field parameters with values around 10^4 cm^{-1}, which are not reasonable due to the small overlap between the 4f and ligand orbitals. Since the XAS measurements indicated considerable mixing between the 4f and ligand orbitals, the effect of decreasing the Stevens orbital reduction parameter, k, were examined. This parameter corrects the calculated magnetic susceptibility for the decrease in orbital angular momentum due to mixing of the metal orbital with the ligand orbitals. Allowing k to vary during fits of the magnetic susceptibility provided reasonable quality fits over a large range of k values, from 0.55 to 0.95 – suggesting that k has a relatively flat $\chi_\nu{}^2$ profile – but often provided unrealistically large crystal field parameters. Hence, the value of k was set to 0.7 based on the n_f value determined by fitting the L_3-edge data using the relationship $k = 1 - n_f$. This provided reasonable crystal field parameters with magnitudes on the order of 10^3 cm^{-1}, which agree well with those reported previously by optical spectroscopy and magnetic measurements (Table 1).[98,99]

Fig. 6 compares the energies of the low-lying $4f^6$ states calculated by CONDON 3 during the fit to the energies of the free-ion states, which were determined by setting $B_0{}^2$, $B_0{}^4$, $B_0{}^6$, and $B_6{}^6$ to small values. Using Fig. 6, one can understand both the magnetic behavior of Cp'_3Eu and why the free ion model fails to reproduce the magnetic susceptibility. In the absence of a crystal field, the energy of the first excited state, $^7F_1$, is 378 cm^{-1} above the ground state, $^7F_0$. The crystal field splits $^7F_1$. The $m_J = \pm 1$ doublet state is destabilized, and the $m_J = 0$ singlet state is stabilized such that it is only 25 cm^{-1} above the ground state. Because the first excited state is at low energy, the value of χ_{TIP} is much larger than it is in the free ion (χ_{TIP} is inversely

Table 1 Values of parameters used to fit the magnetic susceptibility of Cp'_3Eu

	Model	
Parameter	Atomic	Crystal field
k		0.7[a]
l (cm^{-1})	14	223[a]
$n_f(1-k)$	0	0.3
$B_0{}^2$ (cm^{-1})		−2710
$B_0{}^4$ (cm^{-1})		2349
$B_0{}^6$ (cm^{-1})		1917
$B_6{}^6$ (cm^{-1})		−5970
$\chi_n{}^{2b}$	6.9	0.0021

[a] Fixed parameter.

[b] $\chi_\nu{}^2 = \frac{1}{(\text{num. of data} - \text{num. of parameters})}\sum_i \frac{(\chi_{meas} - \chi_{calc})^2}{(\chi_{meas})^2}$.

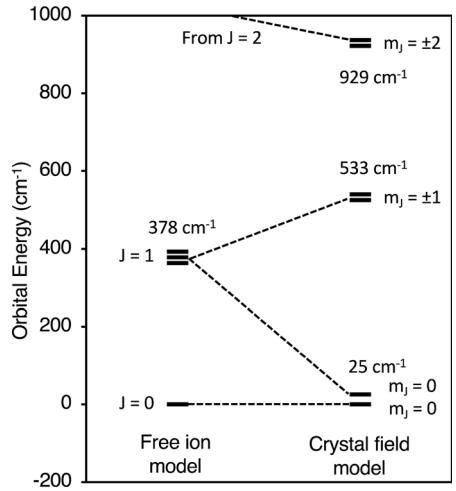

Fig. 6 Low lying states of Cp'_3Eu described using an atomic model and a crystal field model with $k = 0.7$.

proportional to the energy gap). In addition, because the first excited state is at low energy, it becomes thermally populated at low temperatures, which results in a rapid decrease in the magnetic susceptibility of Cp'_3Eu as the temperature increases above ~10 K. In the free ion model (eqn (4)–(6)), the only way to decrease the energy of the first excited state is to decrease λ to a small value, which is not physically meaningful. Even this is not sufficient to model the magnetic susceptibility since the first excited state in the free ion model is a triplet while the first excited state is actually a singlet.

The fact that reasonable values of B_0^2, B_0^4, B_0^6, and B_6^6 could only be obtained when $k \leq 0.75$ indicates that a large degree of orbital mixing is present in Cp'_3Eu. The nature of this interaction can be evaluated from the experimentally derived MO diagram shown in Fig. 7, which was determined by using the crystal field parameters to calculate the splitting of the 4f orbitals. The MO diagram for Cp'_3Eu resembles that previously reported for Cp'_3Nd (ref. 100) and the qualitative MO diagram shown in Fig. 1. In these cases, one 4f-orbital is more strongly destabilized due to interaction with the ligands, and the other six 4f orbitals are similar in energy suggesting little interaction with the ligand orbitals.

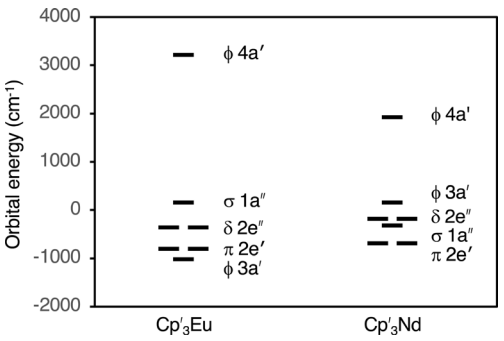

Fig. 7 Experimentally derived MO diagram showing the valence 4f-orbitals for Cp'_3Eu and Cp'_3Nd.

The results from fitting the magnetic susceptibility also illustrate a drawback of this technique, which is that the crystal field model used by CONDON 3 may have multiple sets of parameters that can fit the data well. For this reason, it is helpful to have results from other physical measurements to better constrain the fit. Ideally, one would like to include the energies of the excited states and fit those along with the magnetic susceptibility. Here, we have adopted a different approach and have used the value of n_f determined from XAS measurements to determine the value of k in the crystal field model, 0.7.

Conclusion

In summary, the X-ray spectroscopic and magnetic measurements described above have demonstrated how 4f orbital mixing can increase the magnetic susceptibility of a trivalent Eu organometallic complex, Cp'_3Eu Despite inducing very different core-hole potentials, the C K-edge, Eu $M_{5,4}$-edge, and Eu L_3-edge XAS measurements each provided evidence for C 2p and Eu 4f orbital mixing. The C K-edge XAS and TDDFT calculations also showed that C 2p and Eu 4f orbital mixing occurs specifically in the orbitals of a′ symmetry (4f–π). The amount of charge transfer was expressed using a CI model in terms of the relative contribution of the $|4f^7\underline{L}\rangle$ configuration to the total ground-state wavefunction. The amount of charge transfer determined by fitting of the Eu L_3-edge spectrum, 0.28(4), was used to determine the Stevens orbital reduction parameter, k, used in the modeling of the magnetic susceptibility data. The results of crystal field modeling show that the increased magnetic susceptibility of Cp'_3Eu at low temperature is due to the presence of a low-lying $m_J = 0$ excited state resulting from the splitting of the $^7F_1$ term. The qualitative MO diagram produced by modeling the magnetic susceptibility data is in excellent agreement with the results of the XAS studies.

In the closely related molecule Cp_3Yb, the presence of orbital mixing in Cp_3Yb is manifested by a 12% contribution of the Yb^{2+} charge transfer configuration ($4f^{14}\underline{L}$) to the ground-state, with the remaining 88% from the ionic, Yb^{3+} configuration ($4f^{13}$).[39] The enhancement in charge transfer for Cp'_3Eu compared to Cp_3Yb is consistent with predictions by Denning and coworkers[39] based on the 0.44 eV lower energy of the ligand to metal charge transfer transition for Eu^{3+} *vs.* Yb^{3+}.[44] It is also likely to be a general result when comparing isomorphous Eu^{3+} and Yb^{3+} complexes owing to the lower reduction potential for Eu^{3+} (−0.34 V) compared with Yb^{3+} (−1.05 V) ions.[101] To explore the limits of this trend, we are currently studying complexes with the related ions Sm^{3+} and Tm^{3+}, as well as Nd^{3+} and Dy^{3+}, which may be able to access either $4f^{n+1}$ or $4f^n5d^1$ charge transfer configurations depending on the coordination environment.[58,102]

Data availability

The data supporting this article have been included as part of the ESI.†

Author contributions

Conceptualization and project administration: S. G., Y. Q., P. S., C. B., W. D., W. E., W. L., S. M. Formal analysis: S. G., Y. Q., P. S., L. M., C. B., W. D., W. E., W. L., S. M. Investigation: S. G., Y. Q., P. S., A. D., L. M., T. S., C. B., W. D., W. L., S. M. Resources: S. C., D. H., W. E. Validation: S. G., P. S. Funding acquisition and supervision: P. A., C. B., W. D., W. E., W. L., S. M. Writing – original draft: S. G., Y. Q., P. S., W. L., S. M. Writing – reviewing & editing: all authors.

Conflicts of interest

There are no conflicts to declare.

Acknowledgements

We would like to thank the late Prof. Richard A. Andersen for contributing to the conceptualization of this project. This research was supported at LBNL by the Director, Office of Science, Office of Basic Energy Sciences, Division of Chemical Sciences, Geosciences, and Biosciences (CSGB), U.S. Department of Energy (DOE) under contract no. DE-AC02-05CH11231. Ciccone, Huh, and Evans acknowledge the U. S. National Science Foundation for support of this research under CHE-2154255. This research used resources of the ALS, which is a U.S. DOE Office of Science User Facility under contract no. DEAC02-05CH11231 at LBNL. STXM research described in this paper was conducted at Advanced Light Source Beamline 11.0.2, which was supported by the Director, Office of Science, Office of Basic Energy Sciences Division of Chemical Sciences, Geosciences, and Biosciences; and the Condensed Phase and Interfacial Molecular Sciences Program of the aforementioned Division of the U.S. Department of Energy at LBNL under Contract No. DE-AC02-05CH11231. Additional STXM research was conducted at the Canadian Light Source, which is supported by the Canada Foundation for Innovation, Natural Sciences and Engineering Research Council of Canada, the University of Saskatchewan, the Government of Saskatchewan, Western Economic Diversification Canada, the National Research Council Canada, and the Canadian Institutes of Health Research. The Stanford Synchrotron Radiation Lightsource is supported by the U.S. Department of Energy, Office of Science, Office of Basic Energy Sciences under contract no. DE-AC02-76SF00515.

Notes and references

1 R. Sessoli and A. K. Powell, *Coord. Chem. Rev.*, 2009, **253**, 2328–2341.
2 J. D. Rinehart and J. R. Long, *Chem. Sci.*, 2011, **2**, 2078–2085.
3 N. F. Chilton, C. A. P. Goodwin, D. P. Mills and R. E. P. Winpenny, *Chem. Commun.*, 2015, **51**, 101–103.
4 K. L. M. Harriman and M. Murugesu, *Acc. Chem. Res.*, 2016, **49**, 1158–1167.
5 M. Briganti, E. Lucaccini, L. Chelazzi, S. Ciattini, L. Sorace, R. Sessoli, F. Totti and M. Perfetti, *J. Am. Chem. Soc.*, 2021, **143**, 8108–8115.
6 N. Mahieu, J. Piatkowski, T. Simler and G. Nocton, *Chem. Sci.*, 2023, **14**, 443–457.
7 A. Ramanathan, J. Kaplan, D. C. Sergentu, J. A. Branson, M. Ozerov, A. I. Kolesnikov, S. G. Minasian, J. Autschbach, J. W. Freeland, Z. G. Jiang, M. Mourigal and H. S. La Pierre, *Nat. Commun.*, 2023, **14**, 1–11.
8 U. J. Williams, B. D. Mahoney, P. T. DeGregorio, P. J. Carroll, E. Nakamaru-Ogiso, J. M. Kikkawa and E. J. Schelter, *Chem. Commun.*, 2012, **48**, 5593–5595.
9 L. Ungur, J. J. Le Roy, I. Korobkov, M. Murugesu and L. F. Chibotaru, *Angew. Chem., Int. Ed.*, 2014, **53**, 4413–4417.
10 F. Gendron, B. Pritchard, H. Bolvin and J. Autschbach, *Dalton Trans.*, 2015, **44**, 19886–19900.
11 F.-S. Guo, B. M. Day, Y.-C. Chen, M.-L. Tong, A. Mansikkamäki and R. A. Layfield, *Angew. Chem., Int. Ed.*, 2017, **56**, 11445–11449.
12 C. A. P. Goodwin, F. Ortu, D. Reta, N. F. Chilton and D. P. Mills, *Nature*, 2017, **548**, 439–442.
13 G. M. Risica, V. Vieru, B. O. Wilkins, T. P. Latendresse, J. H. Reibenspies, N. S. Bhuvanesh, G. P. Wylie, L. F. Chibotaru and M. Nippe, *Angew. Chem., Int. Ed.*, 2020, **59**, 13335–13340.
14 M. Tricoire, L. Münzfeld, J. Moutet, N. Mahieu, L. La Droitte, E. Moreno-Pineda, F. Gendron, J. D. Hilgar, J. D. Rinehart, M. Ruben, B. Le Guennic, O. Cador, P. W. Roesky and G. Nocton, *Chem.–Eur. J.*, 2021, **27**, 13558–13567.
15 L. Münzfeld, M. Dahlen, A. Hauser, N. Mahieu, S. K. Kuppusamy, J. Moutet, M. Tricoire, R. Köppe, L. La Droitte, O. Cador, B. Le Guennic, G. Nocton, E. Moreno-Pineda, M. Ruben and P. W. Roesky, *Angew. Chem., Int. Ed.*, 2023, **62**, e202218107.
16 T. Jo and A. Kotani, *Phys. Rev. B*, 1988, **38**, 830–833.
17 J. M. Veauthier, E. J. Schelter, C. J. Kuehl, A. E. Clark, B. L. Scott, D. E. Morris, R. L. Martin, J. D. Thompson, J. L. Kiplinger and K. D. John, *Inorg. Chem.*, 2005, **44**, 5911–5920.
18 C. H. Booth, M. D. Walter, M. Daniel, W. W. Lukens and R. A. Andersen, *Phys. Rev. Lett.*, 2005, **95**, 267202.
19 C. H. Booth, M. D. Walter, D. Kazhdan, Y.-J. Hu, W. W. Lukens, E. D. Bauer, L. Maron, O. Eisenstein and R. A. Andersen, *J. Am. Chem. Soc.*, 2009, **131**, 6480–6491.
20 C. H. Booth, D. Kazhdan, E. L. Werkema, M. D. Walter, W. W. Lukens, E. D. Bauer, Y.-J. Hu, L. Maron, O. Eisenstein, M. Head-Gordon and R. A. Andersen, *J. Am. Chem. Soc.*, 2010, **132**, 17537–17549.
21 G. Nocton, C. H. Booth, L. Maron and R. A. Andersen, *Organometallics*, 2013, **32**, 5305–5312.
22 D. Sergentu, C. Booth and J. Autschbach, *Chem.–Eur. J.*, 2021, **27**, 7239–7251.
23 N. Magnani, *Int. J. Quantum Chem.*, 2014, **114**, 755–759.
24 S. C. Bart, F. W. Heinemann, C. Anthon, C. Hauser and K. Meyer, *Inorg. Chem.*, 2009, **48**, 9419–9426.

25 I. Castro-Rodriguez, K. Olsen, P. Gantzel and K. Meyer, *J. Am. Chem. Soc.*, 2003, **125**, 4565–4571.
26 D. P. Mills, F. Moro, J. McMaster, J. van Slageren, W. Lewis, A. J. Blake and S. T. Liddle, *Nat. Chem.*, 2011, **3**, 454–460.
27 D. M. King, F. Tuna, J. McMaster, W. Lewis, A. J. Blake, E. J. L. McInnes and S. T. Liddle, *Angew. Chem., Int. Ed.*, 2013, **52**, 4921–4924.
28 K. R. Meihaus and J. R. Long, *Dalton Trans.*, 2015, **44**, 2517–2528.
29 V. Mougel, L. Chatelain, J. Pécaut, R. Caciuffo, E. Colineau, J.-C. Griveau and M. Mazzanti, *Nat. Chem.*, 2012, **4**, 1011–1017.
30 Y. Hinatsu, M. Itoh and N. Edelstein, *J. Solid State Chem.*, 1997, **132**, 337–341.
31 Y. Hinatsu, M. Wakeshima, N. Edelstein and I. Craig, *J. Solid State Chem.*, 1999, **144**, 20–24.
32 L. A. Solola, A. V. Zabula, W. L. Dorfner, B. C. Manor, P. J. Carroll and E. J. Schelter, *J. Am. Chem. Soc.*, 2017, **139**, 2435–2442.
33 A. R. Willauer, C. T. Palumbo, F. Fadaei-Tirani, I. Zivkovic, I. Douair, L. Maron and M. Mazzanti, *J. Am. Chem. Soc.*, 2020, **142**, 5538–5542.
34 M. J. Daum, A. Ramanathan, A. I. Kolesnikov, S. Calder, M. Mourigal and H. S. La Pierre, *Phys. Rev. B*, 2021, **103**, L121109.
35 Y. S. Qiao, H. L. Yin, L. M. Moreau, R. L. Feng, R. F. Higgins, B. C. Manor, P. J. Carroll, C. H. Booth, J. Autschbach and E. J. Schelter, *Chem. Sci.*, 2021, **12**, 3558–3567.
36 A. Ramanathan, E. D. Walter, M. Mourigal and H. S. La Pierre, *J. Am. Chem. Soc.*, 2023, **145**, 17603–17612.
37 W. W. Lukens, Jr., S. G. Minasian and C. H. Booth, *Chem. Sci.*, 2023, **14**, 12784–12795.
38 G. Depaoli, U. Russo, G. Valle, F. Grandjean, A. F. Williams and G. J. Long, *J. Am. Chem. Soc.*, 1994, **116**, 5999–6000.
39 M. Coreno, M. de Simone, R. Coates, M. S. Denning, R. G. Denning, J. C. Green, C. Hunston, N. Kaltsoyannis and A. Sella, *Organometallics*, 2010, **29**, 4752–4755.
40 R. G. Denning, J. Harmer, J. C. Green and M. Irwin, *J. Am. Chem. Soc.*, 2011, **133**, 20644–20660.
41 W. W. Lukens, N. Magnani and C. H. Booth, *Inorg. Chem.*, 2012, **51**, 10105–10110.
42 G. Nocton, W. W. Lukens, C. H. Booth, S. S. Rozenel, S. A. Medling, L. Maron and R. A. Andersen, *J. Am. Chem. Soc.*, 2014, **136**, 8626–8641.
43 B. M. Day, F.-S. Guo and R. A. Layfield, *Acc. Chem. Res.*, 2018, **51**, 1880–1889.
44 P. Dorenbos, *J. Phys.: Condens. Matter*, 2003, **15**, 8417.
45 M. T. Trinh, J. C. Wedal and W. J. Evans, *Dalton Trans.*, 2021, **50**, 14384–14389.
46 X. Cao and M. Dolg, *J. Mol. Struct.*, 2002, **581**, 139–147.
47 S. D. Ramarao, A. K. Singh, U. Subbarao and S. C. Peter, *J. Solid State Chem.*, 2020, **281**, 121048.
48 D. N. Huh, J. P. Bruce, S. Ganesh Balasubramani, S. R. Ciccone, F. Furche, J. C. Hemminger and W. J. Evans, *J. Am. Chem. Soc.*, 2021, **143**, 16610–16620.
49 S. G. Minasian, J. M. Keith, E. R. Batista, K. S. Boland, D. L. Clark, S. A. Kozimor, R. L. Martin, D. K. Shuh and T. Tyliszczak, *Chem. Sci.*, 2014, **5**, 351–359.
50 D. E. Smiles, E. R. Batista, C. H. Booth, D. L. Clark, J. M. Keith, S. A. Kozimor, R. L. Martin, S. G. Minasian, D. K. Shuh, S. C. E. Stieber and T. Tyliszczak, *Chem. Sci.*, 2020, **11**, 2796–2809.
51 Y. Qiao, G. Ganguly, C. H. Booth, J. A. Branson, A. S. Ditter, D. J. Lussier, L. M. Moreau, D. R. Russo, D.-C. Sergentu, D. K. Shuh, T. Sun, J. Autschbach and S. G. Minasian, *Chem. Commun.*, 2021, **57**, 9562–9565.
52 M. E. Fieser, M. G. Ferrier, J. Su, E. Batista, S. K. Cary, J. W. Engle, W. J. Evans, J. S. Lezama Pacheco, S. A. Kozimor, A. C. Olson, A. J. Ryan, B. W. Stein, G. L. Wagner, D. H. Woen, T. Vitova and P. Yang, *Chem. Sci.*, 2017, **8**, 6076–6091.
53 J. W. Lauher and R. Hoffmann, *J. Am. Chem. Soc.*, 1976, **98**, 1729–1742.
54 B. E. Bursten and R. J. Strittmatter, *Angew. Chem., Int. Ed.*, 1991, **30**, 1069–1085.
55 L. Maron, O. Eisenstein and R. A. Andersen, *Organometallics*, 2009, **28**, 3629–3635.
56 W. W. Lukens, N. M. Edelstein, N. Magnani, T. W. Hayton, S. Fortier and L. A. Seaman, *J. Am. Chem. Soc.*, 2013, **135**, 10742–10754.
57 T. A. Albright, J. K. Burdett and M. Whangbo, *Orbital Interactions in Chemistry*, John Wiley and Sons, New York, 1985.
58 M. E. Fieser, M. R. MacDonald, B. T. Krull, J. E. Bates, J. W. Ziller, F. Furche and W. J. Evans, *J. Am. Chem. Soc.*, 2015, **137**, 369–382.
59 S. G. Minasian, E. R. Batista, C. H. Booth, D. L. Clark, J. M. Keith, S. A. Kozimor, W. W. Lukens, R. L. Martin, D. K. Shuh, S. C. E. Stieber, T. Tylisczcak and X.-d. Wen, *J. Am. Chem. Soc.*, 2017, **139**, 18052–18064.
60 S. G. Minasian, J. M. Keith, E. R. Batista, K. S. Boland, S. A. Kozimor, R. L. Martin, D. K. Shuh, T. Tyliszczak and L. J. Vernon, *J. Am. Chem. Soc.*, 2013, **135**, 14731–14740.
61 E. Ruhl and A. P. Hitchcock, *J. Am. Chem. Soc.*, 1989, **111**, 5069–5075.
62 A. T. Wen and A. P. Hitchcock, *Can. J. Chem.*, 1993, **71**, 1632–1644.
63 A. T. Wen, E. Ruhl and A. P. Hitchcock, *Organometallics*, 1992, **11**, 2559–2569.
64 A. Bianconi, A. Marcelli, H. Dexpert, R. Karnatak, A. Kotani, T. Jo and J. Petiau, *Phys. Rev. B*, 1987, **35**, 806–812.
65 H. Dexpert, R. C. Karnatak, J. M. Esteva, J. P. Connerade, M. Gasgnier, P. E. Caro and L. Albert, *Phys. Rev. B*, 1987, **36**, 1750–1753.
66 G. Kaindl, G. Schmiester, E. V. Sampathkumaran and P. Wachter, *Phys. Rev. B*, 1988, **38**, 10174–10177.
67 B. T. Thole, G. van der Laan, J. C. Fuggle, G. A. Sawatzky, R. C. Karnatak and J. M. Esteva, *Phys. Rev. B*, 1985, **32**, 5107–5118.
68 G. Kaindl, G. Kalkowski, W. D. Brewer, B. Perscheid and F. Holtzberg, *J. Appl. Phys.*, 1984, **55**, 1910–1915.

69 M. Stavinoha, J. A. Cooley, S. G. Minasian, T. M. McQueen, S. M. Kauzlarich, C. L. Huang and E. Morosan, *Phys. Rev. B*, 2018, **97**, 195146.
70 B. T. Thole, G. Vanderlaan, J. C. Fuggle, G. A. Sawatzky, R. C. Karnatak and J. M. Esteva, *Phys. Rev. B*, 1985, **32**, 5107–5118.
71 J. B. Goedkoop, B. T. Thole, G. van der Laan, G. A. Sawatzky, F. M. F. de Groot and J. C. Fuggle, *Phys. Rev. B*, 1988, **37**, 2086–2093.
72 M. W. Löble, J. M. Keith, A. B. Altman, S. C. E. Stieber, E. R. Batista, K. S. Boland, S. D. Conradson, D. L. Clark, J. Lezama Pacheco, S. A. Kozimor, R. L. Martin, S. G. Minasian, A. C. Olson, B. L. Scott, D. K. Shuh, T. Tyliszczak, M. P. Wilkerson and R. A. Zehnder, *J. Am. Chem. Soc.*, 2015, **137**, 2506–2523.
73 T. A. Pham, A. B. Altman, S. C. E. Stieber, C. H. Booth, S. A. Kozimor, W. W. Lukens, D. T. Olive, T. Tyliszczak, J. Wang, S. G. Minasian and K. N. Raymond, *Inorg. Chem.*, 2016, **55**, 9989–10002.
74 M. G. Silly, S. Blanchandin, F. Sirotti, F. Lux, S. Chevreux, G. Lemercier and F. Charra, *J. Phys. Chem. C*, 2013, **117**, 9766–9771.
75 A. Kotani and H. Ogasawara, *J. Electron Spectrosc. Relat. Phenom.*, 1992, **60**, 257–299.
76 C. Dallera, K. Giarda, G. Ghiringhelli, A. Tagliaferri, L. Braicovich and N. B. Brookes, *Phys. Rev. B*, 2001, **64**, 153104.
77 C. Dallera, M. Grioni, A. Shukla, G. Vankó, J. L. Sarrao, J. P. Rueff and D. L. Cox, *Phys. Rev. Lett.*, 2002, **88**, 196403.
78 S. M. Butorin, A. Modin, J. R. Vegelius, K. O. Kvashnina and D. K. Shuh, *J. Phys. Chem. C*, 2016, **120**, 29397–29404.
79 K. O. Kvashnina, P. M. Kowalski, S. M. Butorin, G. Leinders, J. Pakarinen, R. Bès, H. J. Li and M. Verwerft, *Chem. Commun.*, 2018, **54**, 9757–9760.
80 K. O. Kvashnina and S. M. Butorin, *Chem. Commun.*, 2022, **58**, 327–342.
81 E. Stavitski and F. M. F. de Groot, *Micron*, 2010, **41**, 687–694.
82 R. D. Cowan, *Theory of Atomic Structure and Spectra*, University of California Press, 1981.
83 F. M. F. de Groot and A. Kotani, *Core Level Spectroscopy of Solids*, Taylor and Francis, New York, 2008.
84 S. Harder, D. Naglav, C. Ruspic, C. Wickleder, M. Adlung, W. Hermes, M. Eul, R. Pottgen, D. Rego, F. Poineau, K. Czerwinski, R. Herber and I. Nowik, *Chem.–Eur. J.*, 2013, **19**, 12272–12280.
85 W. Liu, L. Liu, Y. Wang, L. Chen, J. A. McLeod, L. Yang, J. Zhao, Z. Liu, J. Diwu, Z. Chai, T. E. Albrecht-Schmitt, G. Liu and S. Wang, *Chem.–Eur. J.*, 2016, **22**, 11170–11175.
86 K. R. Meihaus, M. E. Fieser, J. F. Corbey, W. J. Evans and J. R. Long, *J. Am. Chem. Soc.*, 2015, **137**, 9855–9860.
87 Y. Takikawa, S. Ebisu and S. Nagata, *J. Phys. Chem. Solids*, 2010, **71**, 1592–1598.
88 M. Andruh, E. Bakalbassis, O. Kahn, J. C. Trombe and P. Porcher, *Inorg. Chem.*, 1993, **32**, 1616–1622.
89 G. S. Ofelt, *J. Chem. Phys.*, 1963, **38**, 2171–2180.
90 J. H. Van Vleck, *The Theory of Electric and Magnetic Susceptibilities*, Oxford University Press, 1932.
91 M.-L. Sun, J. Zhang, Q.-P. Lin, P.-X. Yin and Y.-G. Yao, *Inorg. Chem.*, 2010, **49**, 9257–9264.
92 Y. Wan, L. Zhang, L. Jin, S. Gao and S. Lu, *Inorg. Chem.*, 2003, **42**, 4985–4994.
93 J. Lhoste, A. Pérez-Campos, N. Henry, T. Loiseau, P. Rabu and F. Abraham, *Dalton Trans.*, 2011, **40**, 9136–9144.
94 J. Legendziewicz, V. Tsaryuk, V. Zolin, E. Lebedeva, M. Borzechowska and M. Karbowiak, *New J. Chem.*, 2001, **25**, 1037–1042.
95 C. Benelli, A. Caneschi, D. Gatteschi, L. Pardi, P. Rey, D. P. Shum and R. L. Carlin, *Inorg. Chem.*, 1989, **28**, 272–275.
96 X.-J. Wang, Z.-M. Cen, Q.-L. Ni, X.-F. Jiang, H.-C. Lian, L.-C. Gui, H.-H. Zuo and Z.-Y. Wang, *Cryst. Growth Des.*, 2010, **10**, 2960–2968.
97 M. Speldrich, J. van Leusen and P. Kögerler, *J. Comput. Chem.*, 2018, **39**, 2133–2145.
98 S. Jank, H. Reddmann and H. D. Amberger, *J. Alloys Compd.*, 1997, **250**, 387–390.
99 P. W. Smith, J. Hrubý, W. J. Evans, S. Hill and S. G. Minasian, *J. Am. Chem. Soc.*, 2024, **146**(9), 5781–5785.
100 W. W. Lukens, M. Speldrich, P. Yang, T. J. Duignan, J. Autschbach and P. Kögerler, *Dalton Trans.*, 2016, **45**, 11508–11521.
101 S. Cotton, *Lanthanide and Actinide Chemistry*, John Wiley and Sons, West Sussex, UK, 2006.
102 M. E. Fieser, C. T. Palumbo, H. S. La Pierre, D. P. Halter, V. K. Voora, J. W. Ziller, F. Furche, K. Meyer and W. J. Evans, *Chem. Sci.*, 2017, **8**, 7424–7433.